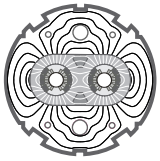

LHC Project Note 410

February 6, 2008

Andres.Gomez.Alonso@cern.ch

Impact Distribution of the Beam Losses at the LHC Collimators in Case of Magnet Failures

Andrés Gómez Alonso, AB/CO-MI, CERN

Keywords: protection systems, magnet failure, collimator, impact distribution

Summary

During LHC operation, magnet failures may affect the beam optics leading to proton losses in the collimators. These losses, with about 360MJ of stored energy per beam at nominal collision operation, are potentially dangerous for the accelerator equipment. The LHC Machine Protection Systems ensure that the beam is extracted safely before these losses can produce any damage. As a magnet failure develops, so does the distribution of the lost particles, longitudinally along the ring as well as transversally at each collimator. The transversal impact distributions of lost particles at the most affected collimators and their evolution with time have been studied for representative magnet failures in the LHC. It has been found that the impact distribution at a given collimator can be approximated by an exponential function with time-dependent parameters. The average impact parameter ranges from about 7 to 620 μm for the cases studied.

Contents

1 Introduction **1**
1.1 The LHC Protection Systems 1
1.2 The LHC Collimation System 1
1.3 Processing algorithm to estimate quench and damage time constants 2

2 Critical magnet failures **2**

3 Simulation procedure **3**
3.1 Magnetic field change 3
3.2 Initial particle distribution 3
3.3 Loss Recording 4
3.4 Impact distributions for the simulated failures 5

4 Simple fit applicable to every impact distributions **6**
4.1 Motivation 6
4.2 Considered functions 8

5 Conclusions **9**

1 Introduction

During the LHC operation at 7 TeV, the energy stored in each beam will be of the order of 360 MJ. At this energy, estimations point that a fraction of 0.01% of the beam could lead to equipment damage and only 10^{-8} of the beam would be enough to produce quenches [1].

1.1 The LHC Protection Systems

In the case of operational irregularities, fast losses can quickly lead to equipment damage. The fastest losses are generated by failures of the kicker magnets used for injection and extraction of the beam [2], [3]. Failures of these elements would lead to a complete loss of the beam in one or a few turns. The fastest failures of LHC magnets excluding kickers would lead to a complete loss of the beam in several tens of turns [4], [5], [6]. As a failure develops, the beam optics are affected and particles start hitting the aperture restrictions in the LHC. If the beam is not extracted in time, these lost particles can lead to equipment damage.

In order to detect the failures and safely extract the beam before any damage is generated by the losses, the LHC Protection Systems are based on different redundant mechanisms [1]. These mechanisms are based on the detection of the failure from the failing equipment itself (failing power converter, quenching magnet, movable object exceedingly restricting the aperture, etc.), which will generate a signal to dump the beam safely before the accelerator optics are even affected [7]. In this case, no or very few losses are expected to happen. In order to add redundancy to these failure detection systems, Beam Loss Monitors (BLMs) distributed along the ring are able to request a beam dump if the losses exceed a certain threshold [8]. For the fastest magnet powering failures, losses may be induced too quickly for the BLMs to request a beam dump before damage levels are reached. In these cases, redundancy is added by Fast Current Change Monitors (FMCMs), which trigger the protection mechanisms in case of fast changes in the current through the magnets [9].

1.2 The LHC Collimation System

The LHC Collimation System has been designed to absorb the steady losses that happen during normal operating conditions. It is composed of blocks of different materials (mainly carbon, copper or tungsten) that restrict the LHC aperture in an staged approach in order to absorb most of the particles that due to large transverse amplitudes would eventually hit the cold aperture [10]. Absorption of these particles in the collimators avoids quenching of the LHC superconducting magnets during steady operation. Collimators susceptible to receive a greater fraction of the beam are made of carbon composites and they can absorb up to about 0.1% of the beam without suffering damage [11].

The LHC Collimation System has been designed to provide a good cleaning efficiency with normal operating conditions [10]. In this case, the following statements are valid:

- Only particles far from the beam axis hit the collimators (those with betatron amplitudes larger than the $6\sigma_{beam}$ primary collimator aperture)

- The average impact parameter is small: from 1.16 to 5.07 μm with injection optics (450 GeV beam energy) and from 0.3 to 1.28 μm with collision optics (7 TeV beam

energy). [10]

- Collimated particles hit first a primary collimator

In the case of magnet failures, lost particles hit collimators first, as they remain the more restrictive aperture limitations. However, the previous statements are not valid:

- All particles could potentially reach the aperture limit if the beam is not extracted in time.

- The average impact parameter can reach up to 620 μm with injection optics and up to 70μm with collision optics.

- Depending on the failure, particles may also hit a secondary collimator first, thus reducing dramatically the cleaning efficiency of the collimation system.

The efficiency of the passive protection provided by the collimation system in case of failure depends also on two factors that do not need to be taken into account when considering beam losses in normal operating conditions: the impact parameter of a collimated particle as well as the type of collimator that it hits first. The study of the distribution of primary losses in the most affected collimators for representative magnet failures at the LHC is presented below.

1.3 Processing algorithm to estimate quench and damage time constants

The motivation behind this study is to set up an efficient algorithm to process data from the simulations of the most critical powering failures during the operation of LHC. With more than 1600 main magnets, the number of critical magnet failures is high. So far, more than 100 failure cases have been considered (each failure case is characterized by the LHC optics and energy, the failing magnet or magnets and the type of failure [4]). Analyzing individually the distribution of lost particles in every single case and its evolution with time is not feasible within reasonable time and effort. Our approach is based on the analysis of representative cases in order to set up an approximation that can be easily obtained from the simulation data and applied automatically to study any failure case.

2 Critical magnet failures

An estimation of the criticality of magnet failures has been presented in [4]. The transversal distribution of the losses in a collimator is related to the time constant of the losses produced by a magnet failure as well as to the type and position of the failing magnet. Particle tracking has been done with several failure cases representative of the whole range of critical magnet failures considered for the LHC. These failure scenarios are listed in table 1, together with the most affected collimator in each case, for which the impact distribution has been studied.

Circuit/Magnet	Failure	Mode	Collimator	σ_{col} [mm]	σ_{inj} [mm]
RD1.LR1	$0V$	Collision	TCP.C6L7.B1	0.278	1.059
RD1.LR1	V_{max}	Injection	TCSG.6R7.B1	0.414	1.577
RQ5.LR7	$0V$	Injection	TCP.B6L7.B1	0.232	0.885
RQ5.LR7	V_{max}	Injection	TCSG.A5L7.B1	0.289	1.101
RD2.L2	Quench	Collision	TCSG.4R6.B1	0.502	1.913
RQX.R1	Quench	Collision	TCSG.A4R7.B1	0.262	0.997
MB.A25R3	Quench	Collision	TCSG.6R7.B1	0.414	1.577

Table 1: Simulated circuits, failures and most affected collimator in each case. OV and V_{max} represent the voltage set by the failing power converter. σ_{col} and σ_{inj} represent the transverse size of the beam at collision and injection respectively, at the location of the most affected collimator.

3 Simulation procedure

The tracking has been performed with MADX introducing a turn-by-turn variable magnetic field. The particles are tracked for a single turn before the lattice values are changed. The time resolution is therefore limited to 1 turn ($89\mu s$), which is enough for the failures considered where the fastest time constants are at least 70 turns (typically, they exceed several hundred turns) [4].

3.1 Magnetic field change

A procedure allowing particle tracking with MADX with an arbitrarily variable magnetic field has been applied to the previous failure scenarios. The change in the magnetic field is governed by the change in the current in the magnet. In the case of a powering failure the power converter sets a voltage across the magnet different to the nominal value and the current in the failing circuit follows an exponential evolution [4]. In the case of a quench, the current decay has been approximated by a half Gaussian [12]. For a quench in MB.A25.R3, only one magnet quenches, but the energy is extracted from the whole circuit by the Quench Protection Systems [13]. In this case the Gaussian decay is applied to the particular quenching magnet, and an exponential current decay is considered simultaneously for the 153 magnets of the circuit RB.A34.

3.2 Initial particle distribution

Because the number of turns while the failure develops can be high, the number of particles that can be simulated in a reasonable time is limited to values between 10^4 and 10^5, depending on the speed of the failure and number of recording locations. The estimated quench limit at 7TeV can be reached if a fraction of losses only about 10^{-8} of the nominal beam intensity reaches the superconducting elements [1].

In order to obtain a good resolution for the very first losses, two particle distributions have been tracked for each failure case: a full Gaussian beam distribution and a Gaussian tail distribution with only the outer 0.1% of the beam. The phase-space distributions of beam 1 at TCP.C6L7.B1 in the horizontal plane for injection and collision are shown in figure 1.

Thus, the obtained resolution for the first lost particles reaches 10^{-7} for 10000 simulated particles, which yields acceptable statistics for the first beam losses produced by the failure. The full distribution is useful to obtain a better understanding of the evolution of the losses in case of failure, even if a complete loss of the beam in the collimators should never happen.

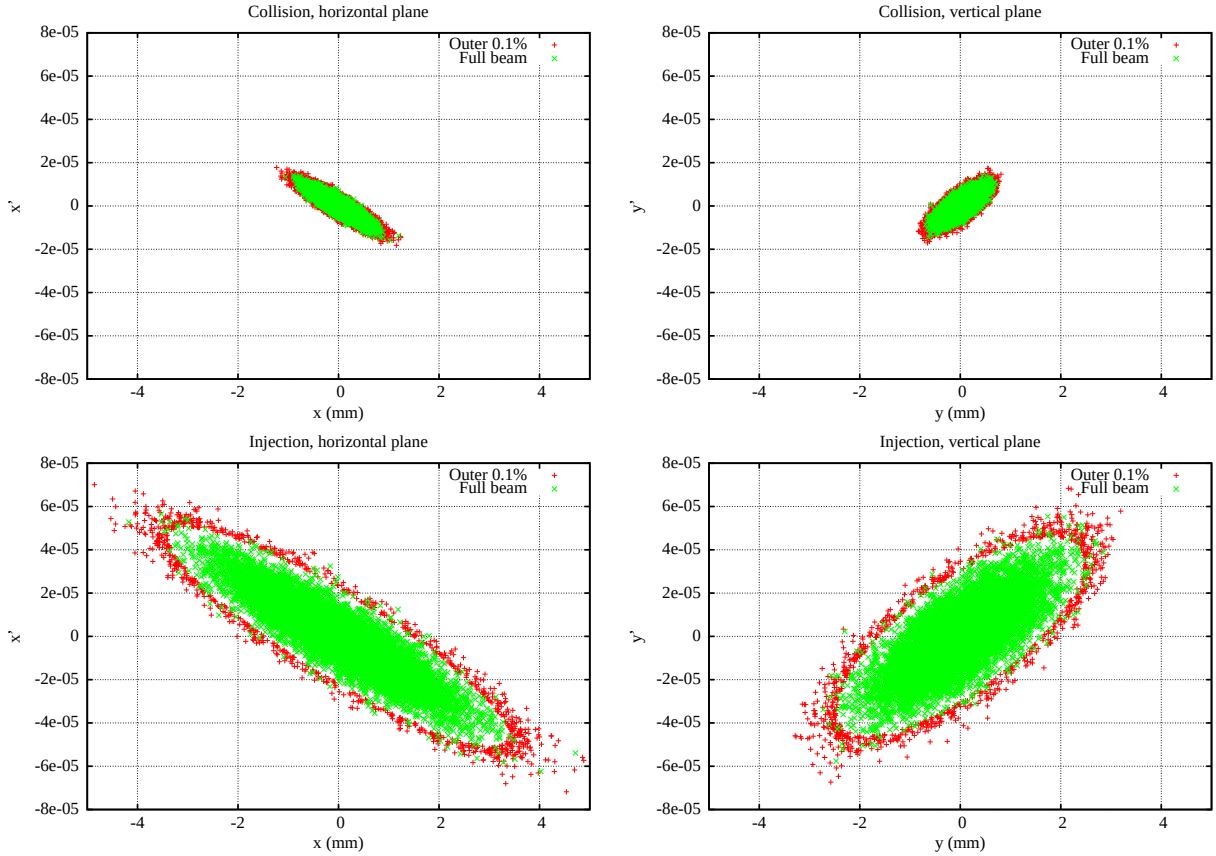

Figure 1: Phase space distributions at the location of TCP.C6L7.B1.

3.3 Loss Recording

During the tracking simulation, the coordinates of the lost particles and the turn are recorded at the location where each particle is lost. It is important to note that only primary losses are recorded. When a particle hits a collimator it can be scattered back into the beam. This fact is not taken into account and the particles hitting a collimator are considered lost.

The interest of recording the primary impact distribution of the particles lies in a later use as input to other simulation codes. It is foreseen to use *colltrack* [14], to estimate the number of scattered particles lost in the cold aperture and *FLUKA* [15] to study the energy deposition in the collimator jaws.

3.4 Impact distributions for the simulated failures

The impact parameter (α) represents the transversal offset of a lost particle in a collimator referred to the edge of the collimator [10]. The distribution of the impact parameters of all the particles lost in the most affected collimator has been generated for the considered failure scenarios. It is named hereafter as the *impact distribution* for a given failure and collimator.

As a failure develops, more and more particles will be lost in the aperture. The time evolution of the primary impact distribution is an important parameter to determine the available time to dump the beam before the quench or damage levels are reached.

Figure 2 shows the impact distribution for the dipole failure cases that were simulated, recorded at the most affected collimators in each case. The width of the impact distribution is strongly dependent on the failure case. In some cases (figures 2e and 2f) the relative amount of losses in each collimator is constant with time. It can also be that the first losses happen at a given collimator, but as the failure develops, more and more particles are lost in another location. In the case of a powering failure of RD1.RL1 setting the failure voltage to its maximum possible value (figures 2c and 2d) the amount of losses recorded at TCP.C6L7.B1 after 30 turns is one order of magnitude greater than at TCSG.6R7.B1. If the failure developed completely (with nominal beam intensity, this should never happen!), the total amount of losses recorded at TCSG.6R7.B1 would be seven times higher than the losses at TCP.C6L7.B1. A similar figure can be observed in the case of a short circuit at RD1.LR1 at collision (figures 2a and 2b).

Another interesting phenomenon can be observed in figure 2f. The impact distribution is truncated at a depth of about 0.2 mm in the collimator. This happens because the particles with orbit excursions big enough to reach greater impact parameters at TCSG.4R6.B1 are intercepted by the collimators upstream (TCDQA.4R6.B1 and TCDQB.4R6.B1).

Figure 3 shows the evolution with time of the total amount of losses recorded in the two particular cases discussed above. The losses at TCSG.4R6.B1 and TCDQB.4R6.B1 (figure 3a) happen at the same time, which is consistent with the data from figure 2f. Figure 3b represents the same picture in the case corresponding to figure 2c and 2d. In this case, the losses at TCP.C6L7.B1 are recorded first, but most particles would hit TCSG.6R7.B1 if the failure developed completely.

Figure 4 shows the impact distribution for the quadrupole failure cases that were simulated, recorded at the most affected collimators in each case. A comparison with figure 2 suggests that the shape of the impact distribution in the case of a quadrupole failure is similar than for losses produced by a dipole failure. The amount of losses recorded on the most affected collimator, however, is smaller in the case of quadrupole failures. This is mainly due to two reasons:

- Quadrupole failures produce more distributed losses than dipole failures.

- The main disturbance on the beam produced by a quadrupole failure is transverse defocusing, which in the absence of other effects leads to symmetric losses in the collimators. Therefore the impact in a jaw is half than in the case of a dipole failure, where all the losses are concentrated in one of the two collimator jaws.

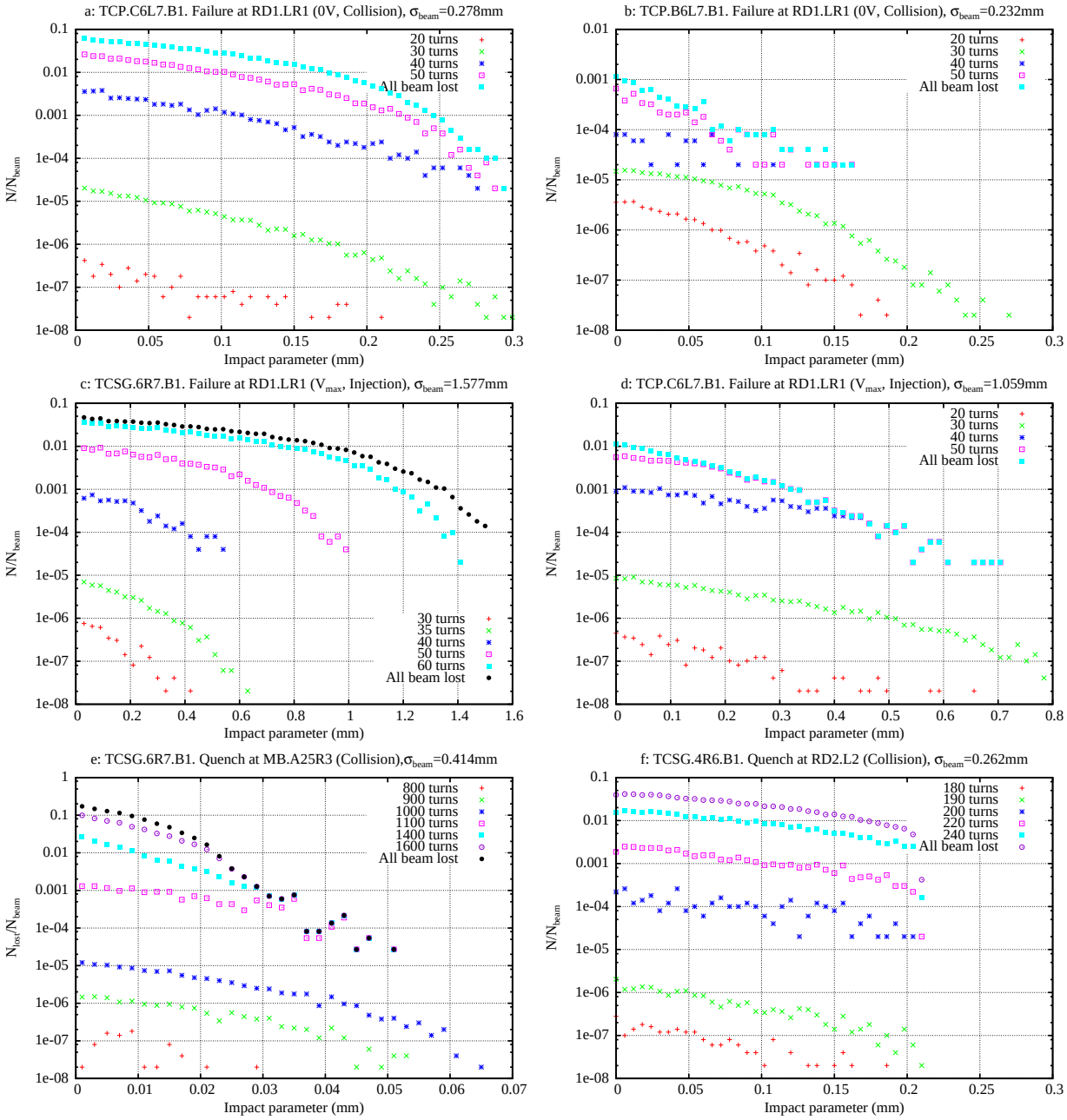

Figure 2: Impact distributions after different numbers of turns for each dipole failure. (a) and (b) represent losses from the same failure scenario recorded at different collimators, as well as (c) and (d).

4 Simple fit applicable to every impact distributions

4.1 Motivation

The distributions presented in figures 2 and 4 show a fast attenuation of the number of particles lost with the impact parameter. To obtain a faster processing of the data for all the

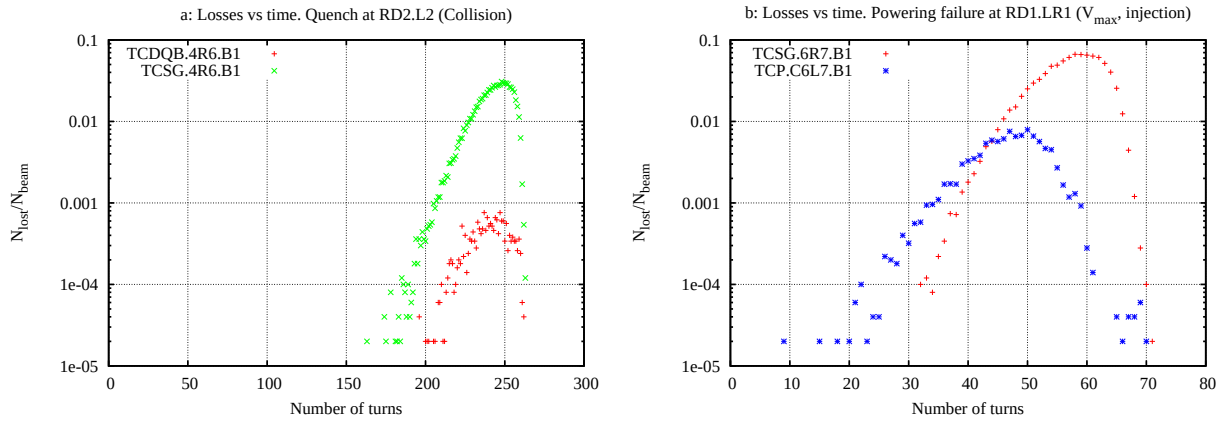

Figure 3: Total number of losses as a function of the number of turns after the failure starts, recorded in different collimators for two failure scenarios: a quench in the D2 left of IP2 (a) and a powering failure of the D1 in IR1 (b)

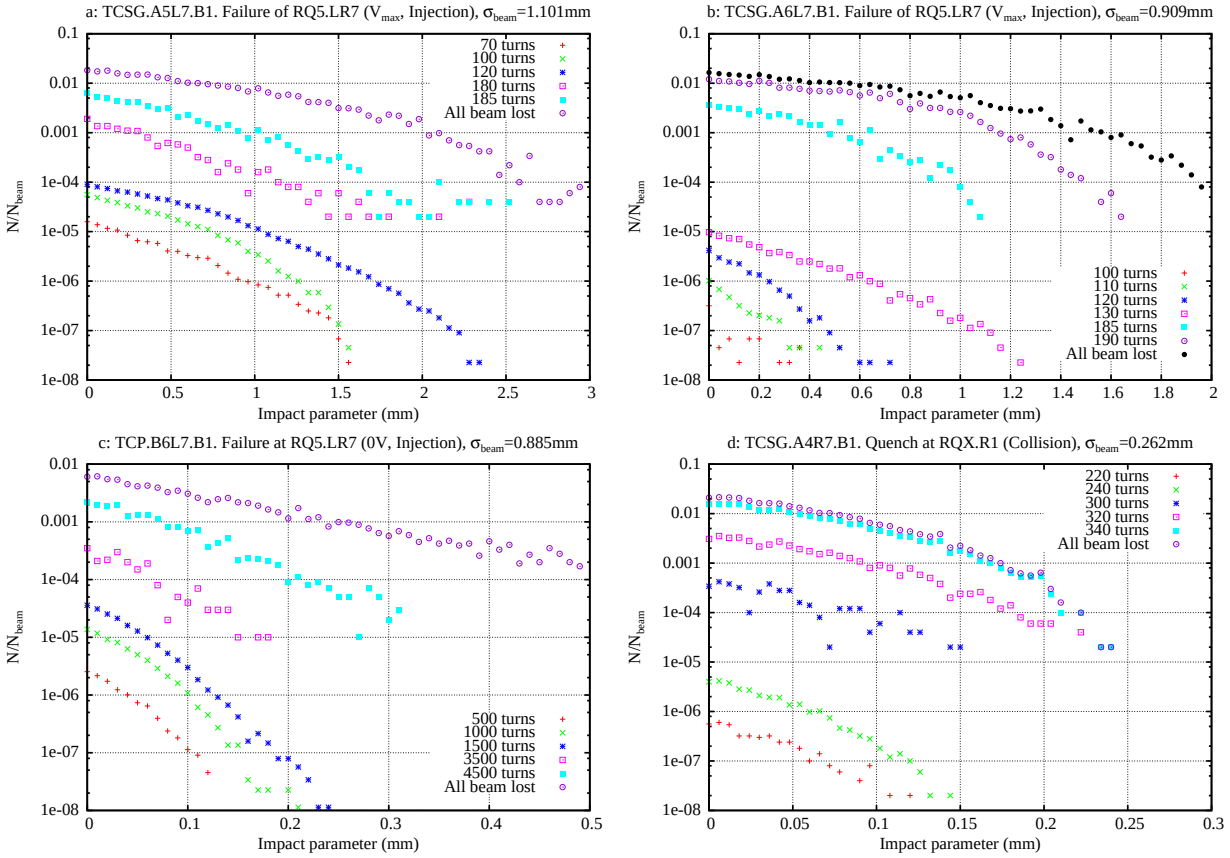

Figure 4: Impact distributions after different numbers of turns for each considered quadrupole failure. (a) and (b) represent losses from the same failure scenario recorded at different collimators.

failures it is more convenient to approximate the impact distribution with a function whose parameters can be obtained directly from the coordinates of the lost particles. This avoids

calculating the distribution every turn, which is a heavy operation in terms of calculation time and memory resources.

With this approach, a reconstruction of the impact distribution can be obtained at any time from only a few stored parameters. This distribution will be used to study the consequences of beam losses, such as the times when quenches or damage would be generated after a failure, and will help to determine appropriate settings for the BLMs for early LHC operation.

4.2 Considered functions

The data presented in the above figures show linear and parabolic trends (in logarithmic scale). The functions $e(x)$, $g(x)$ and $f(x)$ (equation 1) have been evaluated as approximations of the probability density functions (pdf) in three particular failure cases showing impact distributions with different shapes.

$$e(x) = A_e e^{-\frac{x}{\tau_e}} \qquad g(x) = A_g e^{-\frac{x^2}{2\sigma_e{}^2}} \qquad f(x) = A_f e^{-\frac{x^2}{2\sigma^2}-\frac{x}{\tau}} \tag{1}$$

Figure 5a shows a typical impact distribution corresponding to a powering failure of RD1.LR1 at injection (V_{max}) after all the beam is lost (figure 2d). Figure 5b shows an impact distribution after a powering failure of RD1.LR1 at injection (V_{max}) after 35 turns (figure 2c). In this case, the shape of the distribution in logarithmic scale approaches more to a parabola. Figure 5c shows an impact distribution after a quench at MB.A25R3 at collision after 1400 turns (figure 2e). Here the distribution in logarithmic scale is linear, corresponding to an exponential pdf. It has been found that for an a priori unknown distribution following patterns similar to those presented above, $f(x)$ will provide the best fit.

The parameters A_g, σ_g, A_e and τ_e from $e(x)$ and $g(x)$ have been obtained directly from the impact parameter of each lost particle using the method of moments (Appendix A). A direct application of this method for $f(x)$ does not yield a good approximation. From figure 5 we realize that $g(0)$ underestimates the value of the actual pdf at $x = 0$ and that $e(0)$ overestimates it for most of the cases. Besides, $e(0) = g(0) = f(0)$. A better fit is obtained by setting

$$A_f = \frac{A_e + A_g}{2}$$

and applying then applying modified method of moments to obtain σ and τ. Table 2 summarizes the accuracy of the fits for each function in each of the three failure cases studied.

Figure 6 shows the evolution of the parameters A_f, σ and τ with time in the case of a powering failure at RD1.LR1 (V_{max}, injection) recorded at TCP.C6L7.B1. Similar data are obtained for each failure case and collimator, allowing an approximate reconstruction of the impact distribution at any time. Figure 7 shows the reconstructed impact distributions as a function of time for some of the cases presented in figures 3 and 4.

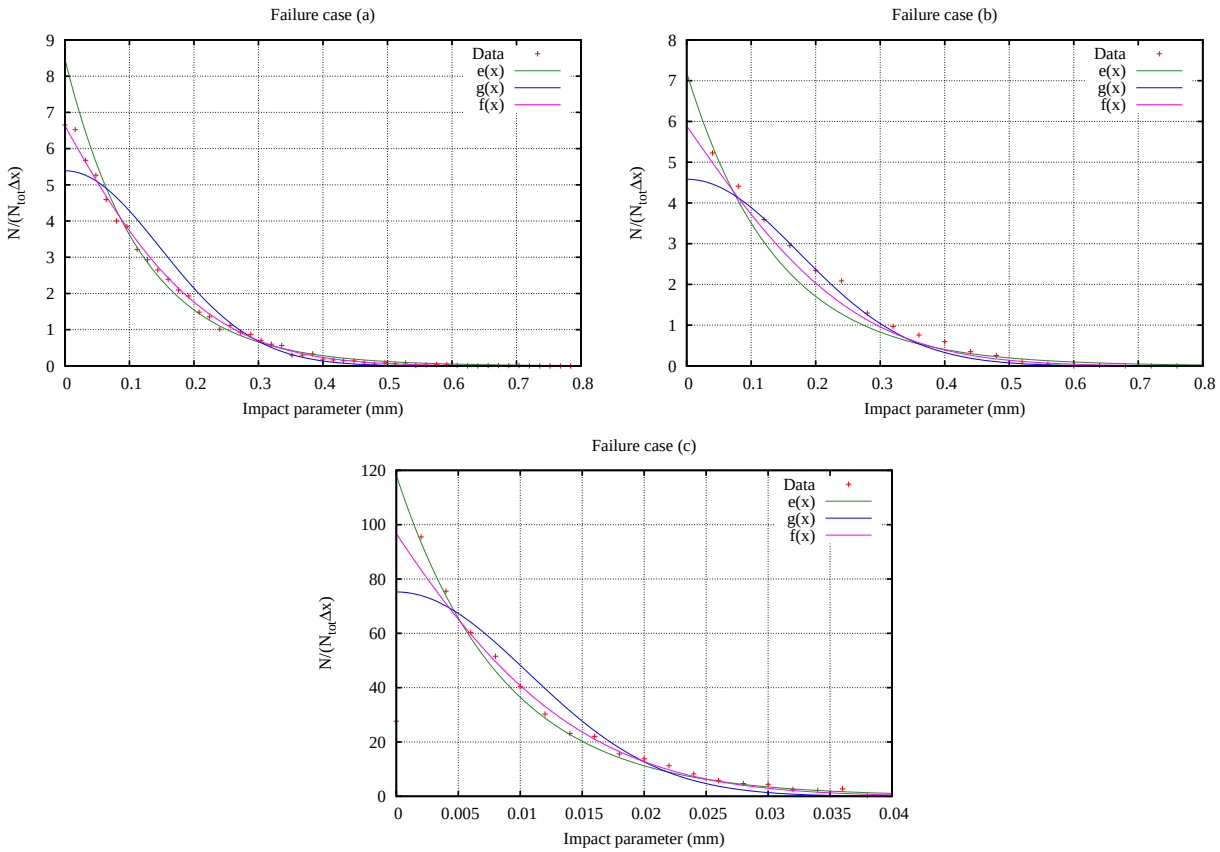

Figure 5: Evaluation of the fits obtained with different types of functions for impact distributions with different shapes. Powering failure of RD1.LR1 at injection (V_{max}) at TCP.C6L7.B1 after all the beam is lost (a). Powering failure of RD1.LR1 at injection (V_{max}) at TCSG.6R7.B1 after 35 turns (b). Quench of MB.A25R3 at collision at TCSG.6R7.B1 after 1400 turns (c). Note that these plots have been normalized so that the integrated probability is equal to 1. The results have to be scaled to the actual number of particles hitting the collimator in each case.

5 Conclusions

In case of failure during the LHC operation, particles are lost in the collimators as the failure develops. The evolution with time of the transverse distribution of these losses in the collimators has been studied through tracking simulations with variable magnetic field using MADX.

The simulations show that in most cases the shape of the impact distribution does not vary significantly with time, and the main change is its amplitude increase (number of lost particles). The impact distribution is smooth in all cases and can be approximated accurately with an exponential function. When the losses are distributed in various collimators the evolution of the impact distribution in one given collimator may not follow a predictable pattern. This is the case of a short circuit at RD1.LR1 at collision energy: after 20 turns the losses at TCP.B6L7.B1 are one order of magnitude greater than at TCP.C6L7.B1, while if all the beam were lost, the losses recorded at TCP.C6L7.B1 would be almost 100 times more

Failure case (a)			
Function	$e(x)$	$g(x)$	$f(x)$
$\frac{\text{RMS of } \Delta y}{f(0)}$	3.26×10^{-2}	5.49×10^{-2}	1.40×10^{-2}

Failure case (b)			
Function	$e(x)$	$g(x)$	$f(x)$
$\frac{\text{RMS of } \Delta y}{f(0)}$	6.04×10^{-2}	3.90×10^{-2}	3.72×10^{-2}

Failure case (c)			
Function	$e(x)$	$g(x)$	$f(x)$
$\frac{\text{RMS of } \Delta y}{f(0)}$	2.37×10^{-2}	6.92×10^{-2}	3.47×10^{-2}

Table 2: Accuracy of the fit for each case of failure studied, referred as in figure 5.

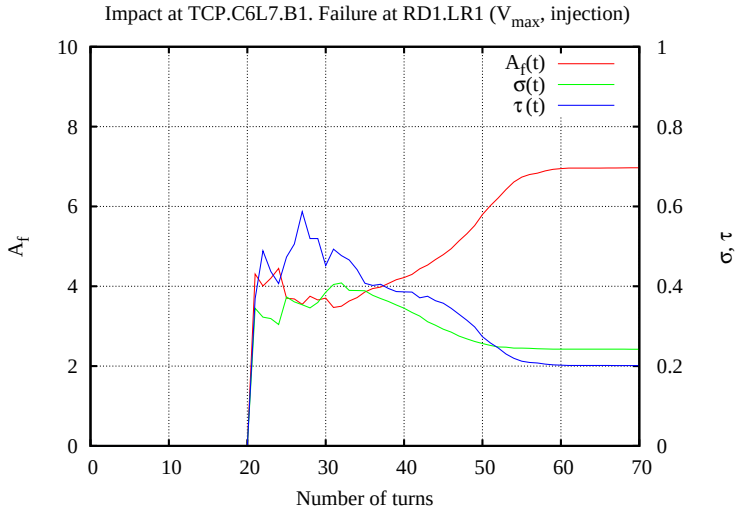

Figure 6: Evolution of the parameters of the fit function with time for a powering failure of RD1.LR1 (V_{max}, injection) recorded at TCP.C6L7.B1.

than at TCP.B6L7.B1. In some other cases, there can be a maximum impact parameter at which the distribution is truncated due to the capture of large amplitude particles by another collimator upstream (Quench at RD2.L2, collision: particles that would hit TCSG.4R6.B1 with an impact parameter greater than 0.21 mm are intercepted by TCDQA.4R6.B1 and TCDQB.4R6.B1). In this case, the truncation remains constant over time.

A general fitting function whose parameters can be obtained directly from the impact parameter of the lost particles has been found. The evolution of the parameters of this function can be stored at each turn and the shape of the impact distribution reconstructed at any given time only from these three parameters.

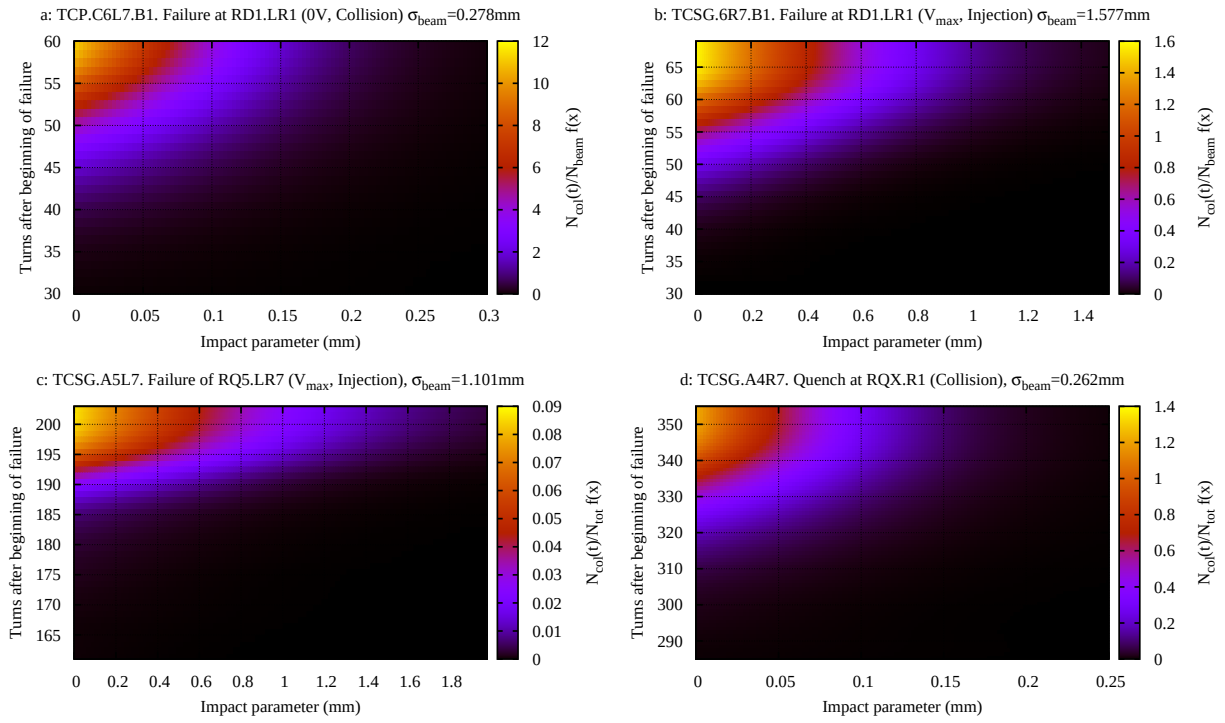

Figure 7: Evolution with time of the reconstructed impact distribution for representative failure scenarios.

References

[1] R. Schmidt and J. Wenninger. Protection against accidental beam losses at the LHC. LHC project report 820, CERN, June 2005.

[2] V. Kain. *Machine Protection and Beam Quality during the LHC Injection Process*. PhD thesis, CERN, 2005.

[3] B. Goddard, R. Assmann, E. Carlier, J. Uythoven, J. Wenninger, and W. Weterings. Protection of the LHC against unsynchronised beam aborts. LHC project report 916, CERN, July 2006.

[4] A. Gómez Alonso. Most probable failures in LHC magnets and time constants of their effects on the beam. LHC project note 389, CERN, November 2006.

[5] V. Kain. Power converter failure of the normal conducting D1 magnet at experiment insertions IR1 and IR5. LHC project note 322, CERN, Sep 2003.

[6] O. Bruning. Mechanisms for beam losses and their time constants. Technical report, CERN, 2001.

[7] B. Todd. *A Beam Interlock System for CERN High Energy Accelerators*. PhD thesis, CERN, 2006.

[8] E. B. Holzer et al. Beam loss monitoring system for the LHC. CERN-AB-2006-009, CERN, Sep 2005.

[9] M.Werner, M.Zerlauth, R.Schmidt, V.Kain, and B.Goddard. A fast magnet current change monitor for machine protection in HERA and the LHC, 10th international conference on accelerator and large experimental physics control systems ICALEPCS 2005. In *Europhysiscs conference abstracts*, volume 29J, 2005.

[10] G. Robert-Demolaize. *Design and Performance Optimization of the LHC Collimation System*. PhD thesis, CERN, 2006.

[11] P. Sievers et al. Appropriate materials for LHC collimators. In *LHC Performance Workshop - Chamonix XII*, 2003.

[12] F. Sonnemann R. Schmidt (dir). *Resistive transition and protection of LHC superconducting cables and magnets*. PhD thesis, CERN, 2001.

[13] K. Dahlerup-Petersen, R. Denz, J.L. Gómez-Costa, D. Hagedorn, P. Proudlock, F. Rodríguez-Mateos, R. Schmidt, and F. Sonnemann. The protection system for the superconducting elements of the large hadron collider at CERN. LHC project report 283, CERN, April 1999.

[14] G. Robert-Demolaize, R. Assmann, S. Redaelli, and F. Schmidt. A new version of sixtrack with collimation and aperture interface. In *Proceedings of 2005 Particle Accelerator Conference, Knoxville, Tennessee*, July 2005.

[15] G. Battistoni, F. Cerutti, A. Fasso, A. Ferrari, S. Muraroi, J. Ranft, S. Roesler, and P.R. Sala. The FLUKA code: description and benchmarking. In *Hadronic Shower Simulations Workshop, Batavia, IL, USA*, September 2006.

[16] Ronald E Walpole, Raymond H Myers, Sharon L Myers, and Keying Ye. *Probability and statistics for engineers and scientists ; 8th ed.* Upper Saddle River, NJ: Pearson, 2007.

APPENDIX A - Adaptation of the method of the moments for the calculation of A_f, σ and τ

The method of the moments [16] is used to estimate the parameters of a probability density function (pdf) from the values of the random variable distributed according to it. The method is based in equating the moments estimated from samples of the random variable with the unobservable population moments, and then solving those equations for the parameters to be estimated.

If f is the pdf of the distribution, its moments of order n are defined by

$$\mu_n = \int_{-\infty}^{\infty} x^n f(x) dx \tag{A-1}$$

An estimation of the n^{th} moment can also be obtained from the samples of the random variable:

$$\mu_n = \frac{1}{N} \sum_{i=1}^{N} x_i^n \tag{A-2}$$

where N is the total number of samples and x_i the value of each sample.

The calculation of the four first moments for $f(x) = A_f e^{-\frac{x^2}{2\sigma} - \frac{x^2}{\tau}}$ yields, after some algebraic manipulations

$$\mu_0 = \frac{A_f \sqrt{\pi} \sigma}{\sqrt{2}} e^{\frac{\sigma^2}{2\tau^2}} erfc\left(\frac{\sigma}{\sqrt{2}\tau}\right) = 1 \tag{A-3}$$

$$\mu_1 = \sigma^2 \left(A_f - \frac{1}{\tau}\mu_0\right) \tag{A-4}$$

$$\mu_2 = \sigma^2 \left(\mu_0 - \frac{1}{\tau}\mu_1\right) \tag{A-5}$$

$$\mu_3 = \sigma^2 \left(\mu_1 - \frac{1}{\tau}\mu_2\right) \tag{A-6}$$

This recurrent relationship among the moments is very convenient: equations A-4, A-5 and A-6 can be analytically solved for A_f, σ and τ, without having to deal with expressions such as A-3. The resolution yields:

$$A_f = \frac{2\mu_1\mu_2 - \mu_1^3 - \mu_3}{\mu_2^2 - \mu_1\mu_3} \tag{A-7}$$

$$\sigma = \sqrt{\frac{\mu_2^2 - \mu_1\mu_3}{\mu_2 - \mu_1^2}} \tag{A-8}$$

$$\tau = \frac{\mu_2^2 - \mu_1\mu_3}{\mu_1\mu_2 - \mu_3} \tag{A-9}$$

However, it has been found that this estimation tends to underestimate $f(x)$ for small values of x. A better result can be obtained if A_f is set to a convenient value and then σ and τ are calculated from A-4 and A-5.

To find an appropriate value for A_f the method of the moments is applied to $g(x) = A_g^{-\frac{x^2}{2\sigma_g}}$ and $e(x) = A_e^{-\frac{x}{\tau_e}}$. This yields:

$$A_e = \frac{1}{\mu_1} \tag{A-10}$$

$$A_g = \frac{2}{\pi\mu_1} \tag{A-11}$$

and setting $A_f = \frac{A_e + A_g}{2}$ we obtain from A-4 and A-5 the expressions that we used to define the parameters for $f(x)$.

$$A_f = \frac{1}{2\mu_1}\left(1 + \frac{2}{\pi}\right) \tag{A-12}$$

$$\sigma = \sqrt{\frac{2\mu_1^2\left(\mu_1^2 - \mu_2\right)}{\frac{2}{\pi}\mu_1^2 - \left(1 + \frac{2}{\pi}\right)\mu_2}} \tag{A-13}$$

$$\tau = \frac{2\mu_1\left(\mu_1^2 - \mu_2\right)}{2\mu_1^2 - \left(1 + \frac{2}{\pi}\right)\mu_2} \tag{A-14}$$